Hybrid organophosphonic-silane coating for corrosion protection of magnesium alloy AZ91: the influence of acid and alkali pre-treatments

Viviane Dalmoro[a,*], Denise S. Azambuja[a], Carlos Alemán[b,c], Elaine Armelin [b,c,*]

[a] *Instituto de Química, Universidade Federal do Rio Grande do Sul Av. Bento Gonçalves 9500 - CEP 91501-970, Porto Alegre, RS, Brazil.*

[b] *Departament d'Enginyeria Química, EEBE, Universitat Politècnica de Catalunya, C/ d'Eduard Maristany, 10-14, Edifici I, E-08019, Barcelona, Spain.*

[c] *Barcelona Research Center in Multiscale Science and Engineering, Universitat Politècnica de Catalunya, Campus Diagonal Besòs (EEBE), C/ d'Eduard Maristany 10-14, Edifici IS, 08019, Barcelona, Spain.*

Corresponding authors: elaine.armelin@upc.edu and viviane.dalmoro@camaqua.ifsul.edu.br

Abstract

This work reports the development of environmentally friendly coatings for the protection against corrosion of AZ91 magnesium alloy substrates. As a novelty, the synergic combination of the use of silica precursors and phosphonic acid molecules has been investigated for first time in the protection of AZ91 Mg alloy. Hybrid films have been prepared by the sol–gel synthesis using tetraethoxysilane (TEOS) and methylmethoxysilane (MTMS), as co-monomers; and 1,2-diaminoethanetetrakismethylenephosphonic acid (EDTPO) and phenylphosphonic acid (PhPA), as adhesion promoter molecules. In order to improve the homogenous deposition of the silica network, several chemical pre-treatments were approached. The highest corrosion resistance, as determined by electrochemical impedance spectroscopy (EIS), has been observed for the AZ91 Mg alloy submitted to a passivation treatment with Na_3PO_4/NaOH, before the sol-gel deposition. Particularly, the addition of low concentrations of EDTPO, which contains four active phosphonic groups, improves considerably the coating's resistance, as demonstrated by EIS, due to the formation of multiple covalent interactions with silica network and the passivated metal substrate.

Keywords: Magnesium alloy; Phosphonic acid; Sol-gel; X-Ray photoelectron spectroscopy; Scanning electron microscopy.

1. Introduction

Mg alloys present remarkable advantages with respect to other alloys, such as, low density, good machinability, high damping capacity and strength/weight ratio, large castability, and excellent recyclability [1–3]. The corrosion resistance of Mg alloys is achieved by imposing very strict limits on three elements: iron, copper and nickel. These are limited to very low levels making it necessary to use primary magnesium in the production of the alloys [4]. On the other hand, Mg alloys are becoming increasingly important materials for applications in which the weight reduction is fundamental, as for example in aircraft, automotive and construction industries, contributing to save energy and to reduce the environmental impact [2,5]; as well as in the biomedical field, in which the biocompatibility and biodegradability must be preserved [6,7].

AZ91 alloy, which is the most widely used Mg die cast alloy, exhibits good corrosion resistance when compared to steel and aluminum alloys [8]. Commercial AZ alloys (Mg-Al-Zn system) contain at about 9 wt.% of Al, and the secondary alloying elements are Zn (0.74 wt.%) and Mn (0.18 wt.%). The Al addition provides better castability and increases of ambient tensile, compressive, and fatigue strength [9] of Mg alloys, whereas also enhances the vulnerability to corrosion. The Zn and Mn provide the optimum combination of strength and lightness [10].

The corrosion resistance of AZ91 has been investigated in several media, like NaCl [8,11–13], and in both acid and basic solutions [14–18]. Furthermore, as AZ91 alloy has been proposed as a biodegradable biomaterial for the production of bioabsorbable medical devices [19], and corrosion resistance studies have also been conducted in natural and artificial body fluids [19–21]. However, the most relevant publications in this field are centered in the AZ31 Mg alloy, with less content of Al elements than AZ91 specimens [6,7]. Analysis of the reactions and mechanisms involved in aluminum-zinc Mg alloys

deterioration [3,9,11–15,22] indicates dependence on the microstructure, pH and, especially, on chloride concentration; the latter being responsible for promoting fast attack, even in neutral aqueous solutions.

Procedures for the corrosion protection of Mg alloys include the employment of high purity or new alloys, rapid solidification processing, isolation of surface from the environment through organic coatings, and surface modification [23,24]. Successful examples of surface modification and the surface isolation are the creation of Mg-Al layered double hydroxide (LDH)-containing $Mg(OH)_2$ film (*i.e.* creation of conversion layers) [3,22,25] and employment of sol-gel films [26–32], respectively. Sol-gel films are particularly attractive because of their low-cost, the simplicity of the coating deposition technique (*e.g.* usually dip-coating), and the use of environmentally friendly solvents (*e.g.* water-ethanol). Nevertheless, the adhesion and formation of a uniform sol-gel film is a critical point due to the inadequate superficial properties of the Mg alloys. Therefore, an appropriate pre-treatment process is necessary to achieve an uniform coating growing and avoid defects and coating failure [18].

In recent years our group has evidenced the excellent performance of sol-gel technology for protecting Al surfaces from corrosion [33–35]. Furthermore, in a pioneering study we proved the synergy between silane molecules and catalytic amounts of phosphonic groups [36]. Thus, the incorporation of phosphonic acid into the sol-gel solution usually results in the formation of an adherent, homogenous and stable silane coating onto the Al alloy surface, improving the protection against corrosion. In addition, we showed that phosphonic groups and silica precursors stablish good adhesion with the Al surface and the organic coating layer [37,38], improving the formation of the silica network and acting as an intermediate coating layer between the metal surface and the outer layer [36].

In this study, we report a novel, environmentally friendly, inexpensive, and simple sol-gel deposition for the *in-situ* formation of a homogenous anticorrosive silane layer, containing organophosphonic molecules, onto AZ91 Mg alloy surfaces. It worth noting that the concomitant uses of phosphonic acids and silica precursors for generating sol-gel films on Mg alloy have not been described previously. Results demonstrate that the addition of organophosphonic acid offers better film forming properties and protection against corrosion than pure organosilane coatings.

2. Experimental procedure

2.1 Materials. Inorganic reagents, sodium phosphate tribasic dodecahydrate (99 %), acetic acid (99.8 %), hydrofluoric acid (48 %) and methyltrimethoxysilane (MTMS, 97%) were purchased from Sigma-Aldrich Co., whereas tetraethoxysilane (TEOS, 98%) was supplied by Merck Group. Phenylphosphonic acid (PhPA) and 1,2-diaminoethanetetrakis methylenephosphonic acid (EDTPO) were purchased from Sigma-Aldrich (98%) and Dojindo-Japan (97%), respectively. All reagents were used without further purification. Organic solvents, acetone and ethanol (Nuclear, 99.5%) were supplied by Panreac S.A. Mg alloy AZ91D disks, hereafter referred as AZ91, with dimensions of 24 mm of diameter and 4 mm of thickness, were used for the electrochemical experiments. The chemical composition of AZ91 magnesium alloy disks was obtained with a calibrated optical emission spectrometer SPECTROMAXx and corresponds to (wt. %): Al 8.83wt.%; Zn 0.66 wt.%; Mn 0.18 wt.%; Si 0.021 wt.%; Cu <0.002 wt.%; Ni <0.001 wt.%; Fe <0.004 wt.%, and balanced Mg.

2.2 Substrate pre-treatments and sol-gel deposition. AZ91 disks were previously sanded with silicon carbide papers (grain size #1200) and, subsequently, thoroughly

washed with distilled water, before the etching processes. Afterwards, one of the three following pre-treatments was applied: (*i*) immersion in a Na_3PO_4 (10 $g \cdot L^{-1}$) / NaOH (50 $g \cdot L^{-1}$) solution (pH 13.9) for 40 min at 60 °C [39]; (*ii*) immersion in 0.05 $mol \cdot L^{-1}$ acetic acid solution (pH 3) for 30 seconds at room temperature (RT)[36][37]; or (*iii*) immersion in hydrofluoric acid (HF) in water (10% v/v, pH -1.8) for 10 min at RT The substrates obtained from the subsequent three pre-treatments have been denoted AZ91 phosphate, AZ91 acetic and AZ91 hydrofluoric, respectively.

Sol-gel solutions were prepared as follows. First, a solution composed by ethanol, deionized water (18.3 MΩ·cm), MTMS and TEOS with 50:46:3:1 volume ratio (v/v) was stirred for 1 hour at RT. This solution was stored, without stirring, for up to 3 days to the complete hydrolysis and condensation of organosilane molecules. Then, the pre-treated AZ91 disks were immersed in the precursor solution for 30 min and placed in a horizontal position on a flat surface inside the oven, at 110 °C for 1 hour, to ensure the silane monolayer deposition and curing processes. The immersion in and removing of samples from the silane solution were carried out carefully, in vertical position, before placement to the oven. Scheme 1 depicts an illustration for the aforementioned processes.

Alternatively, other sol-gel solution containing ethanol, deionized water, TEOS, MTMS and phosphonic acid was prepared and was deposited onto AZ91 surface with the same experimental conditions than the precursor solution. In order to evaluate the influence of the chemical nature of phophonic acids on the adhesion and protection of the Mg alloy surface, two compounds, PhPA and EDTPO, were tried. The volume ratio (v/v) employed for this second sol-gel solution was 50:46:3:1, with ethanol; deionized water; MTMS:TEOS and phosphonic acid; respectively. The concentrations of phosphonic acid assessed, as well as the codification of all reagents used to identify the coatings deposited onto the Mg alloy surfaces, are summarized in the Table 1.

2.3 Characterization. The chemical composition of AZ91 surfaces pre-treated with acid or basic solutions, and coated with an organosilane layer, was determined by X-ray photoelectron spectroscopy (XPS) and energy dispersive X-ray spectroscopy (EDX). XPS analyses were performed in a SPECS system equipped with a high intensity twin anode X-ray source XR50 of Mg/Al (1253 eV/1487 eV) operating at 150 W, placed perpendicular to the analyzer axis, and using a Phoibos 150 MCD-9 XP detector. The X-ray spot size was 650 μm. Samples were fixed mechanically into a special sample holder using a double side tape. The spectra were recorded with a pass energy of 25 eV in 0.1 eV steps at a pressure below 6×10^{-9} mbar. The C 1s peak, with a binding energy of 284.8 eV, was used as an internal reference. The atomic percentage of each element was determined by dividing the peak area of the most intense XPS signal of each element by the corresponding sensitivity factor and expressing it as a fraction of the sum of all normalized peak areas. High resolution XPS spectra were acquired by Gaussian/Lorentzian curve, fitting after S-shape background subtraction, for the following elements: C 1s, O 1s, Mg 2s and 2p, and Si 2p. For bare alloy (AZ91 disk), the surface was first polished, washed three times with isopropanol, ethanol, deionized water and acetone, under ultrasound bath for 5 min, dried under nitrogen flow and vacuum; then *in situ* sputtering (Ar gas), of about 2 min, was applied in the equipment to eliminate the surface contamination by carbon compounds.

The morphology and the chemical composition of the metal surface, with and without silane coatings, were evaluated by scanning electron microscopy (SEM), using a Focused Ion Beam Zeiss Neon 40 scanning electron microscope, equipped with EDX analysis and operating at 30 kV.

The protection imparted by the two adhesion promoters studied in this work, PhPA and EDTPO, was investigated by electrochemical impedance spectroscopy (EIS). EIS analyses were conducted using an AUTOLAB PGSTAT30/FRA2 equipment, in potentiostatic mode and open-circuit potential (OCP). A typical three electrode cell, with a saturated calomel electrode (SCE) as reference electrode, a platinum mesh as counter electrode and magnesium alloy AZ91 disks as working electrode were used. A solution of 0.05 mol L^{-1} NaCl (pH 7), at 25 ± 3 °C, was employed as electrolyte. Electrochemical experiments were performed, at least, in triplicate using an exposed surface area of 1.0 cm^2. Samples were measured in a frequency range of 100 kHz to 10 mHz by applying ± 10 mV sinusoidal wave perturbation versus OCP, being collected 7 points per decade.

3. Results and discussion

3.1 Effect of acid and basic pre-treatments on the morphology and in the electrochemical behavior of AZ91 surfaces

SEM micrographs of the sanded AZ91 surface show the appearance of horizontal marks and some small fragments coming from the mechanically induced metal delamination (Figure 1a-d). However, the metal surface composition was not affected by the mechanical pre-treatment, as was confirmed by EDX (Figure 1e). In opposition, the three chemical pre-treatments applied, altered the composition of the metal surface as well as induced the formation of corrosion products and passivation layers, as expected.

The surface of AZ91 phosphate samples, which correspond to the metal plate pre-treated with Na_3PO_4/NaOH, was slightly attacked. In the SEM micrographs, displayed in the Figure 2a-d, the main marks are still present, even though some precipitates appeared onto the surface. Although the major peaks observed from EDX analyses correspond to Mg, Al and O (Figure 2e), crystalline structures (probably $Mg_3(PO_4)_2$ or Na_3PO_4), were

detected as isolated particles, upper the surface and in the micrometer marks caused by SiC particles. Jiang *et al.* [41] described some arranged lamellar crystals partially covering the surface of Mg-Zn-Zr alloys after immersion in $Ca_3(PO_4)_2$ solution for 45 min, which is in agreement with the results obtained in the present study. In fact, Mg is passivated in alkaline solutions with pH > 11 due to the formation of $Mg(OH)_2$, which is thermodynamically stable in the metal-water Pourbaix diagram [42], while the β phases dissolves. The basic pH of the alkaline solution used in the pre-treatment of AZ91 samples is the responsible for the relatively high concentration of Mg, Al and O detected by EDX analyses (Figure 2e), supporting the formation of $Mg(OH)_2$ and aluminum hydroxides ($Al(OH)_4^-$) and few phosphate crystals inside the pitting areas.

On the other hand, acid pickling usually results in surfaces severely attacked with a large degree of corrosion. Specifically, SEM micrographs of AZ91 acetic samples display a rough and heterogeneous composition (Figures 3a-d). As it can be seen, globular particles, which are identified even at low magnification images, are located in the intergranular zones. Additionally, EDX analysis displayed in the Figure 3e, indicates that whiter areas are mainly Al_2O_3, while darker zones correspond to Mg (82.9%) with scarce oxygen content (3.2%).

When hydrofluoric acid (HF) is employed as chemical pickling agent, many micro-corrosion cells can be formed on the alloy surface due to the potential difference between α and β phases [43]. The microstructures and phase compositions of the as-cast AZ91 alloy is composed of primary α-Mg matrix (α-phase), discontinuous β-$Mg_{17}Al_{12}$ phase (β-phase) and small blocks of α/β-phases (eutectic phase). In these micro-cells, the α phase acts as the micro-anode in which the magnesium metal dissolves, whereas the β phase is the micro-cathode in which hydrogen reduction takes place, resulting in gas emission. According to previous study [39,40,44], the reaction between Mg^{2+} and F^- ions

for the obtaining of insoluble MgF_2 occurs in the metal/solution interface. The MgF_2 formation strongly depends on the HF concentration and pre-treatment time [40]. SEM micrographs (Figure 4a-d), which display thick and highly cracked layers and some particles aggregations, show the severe attack promoted by the HF on AZ91 hydrofluoric samples. The presence of a high content of fluorine and magnesium atoms in the EDX analyses (Figure 4e), at several zones at sample surface, evidences the presence of MgF_2 microscopic layer. Birbilis and co-workers [18] evaluated the effect of different chemical pre-treatments to completely eliminate the Mg β phase from the AZ91 surface. More specifically, those authors checked the influence of H_3PO_4, HNO_3, HCl, citric acid ($C_6H_8O_7$), NaOH and $ZnSO_4$ solutions. Among these aqueous solutions, they concluded that the diluted organic acid, $C_6H_8O_7$, propitiated the less aggressive pitting attack when short exposition times are employed. Overall, results indicate that the Mg alloy can be protected with other materials if the pre-treatment process is well controlled. For this purpose, the following process is recommended: *i)* activation to avoid the formation of β-phase structures; *ii)* creation of a $Mg(OH)_2$ layer by conditioning with hydroxide solutions; and *iii)*, re-activation with citric acid to eliminate such hydroxide stable layer.

The Bode diagrams of the Mg alloy submitted to the three considered pre-treatments and exposed to a chloride solution for 1h and 48 h are depicted in the Figure 5. The Bode profiles show that the pre-treatment has a notable influence in the impedance and phase angle values. After 1h of samples immersion in NaCl, the AZ91 acetic sample exhibited the worst response (Figure 5a), with in the lowest polarization resistance (R_p). For AZ91 hydrofluoric and AZ91 acetic samples, the Bode plots consisted of one-time constant (τ_1), followed by an inductive behavior at frequencies lower than 10^{-1} and $10^{-0,1}$ Hz, respectively. The latter can be attributed to the relaxation of the adsorbed species [*e.g.* $Mg(OH)_{ads}$ or $Mg(OH)_2$] [45] or to the bulk relaxation of species in the oxide layer [46].

The higher impedance modulus values of AZ91 hydrofluoric samples has been attributed to the insoluble MgF_2 layer formed by the pre-treatment with HF (Figure 4), which acts as a barrier against the dissolution of the Mg alloy [39,44].

The EIS results reveal the corrosion susceptibility of the Mg alloy to the chloride medium. The α-Mg matrix and the intermetallic particles, in the eutectic form α + β with lamellar structure, constitute the main AZ91 microstructure, as explained before. The more accepted corrosion mechanism is that where the β phase behaves as a cathode, promoting the localized corrosion of α-phase and the grain boundaries [47]. The Bode diagram recorded for AZ91 phosphate samples presents two time constants. The first one corresponds to the charge transfer process, while the second one is generally associated to the mass transfer in the solid phase [48], which consists of the hydroxide/oxide layers. After 48 h of the samples immersion in NaCl solution, the inductive process remains exclusively in the AZ91 acetic sample. Lastly, the AZ91 surface, pre-treated with HF, suffers changes in the relaxation process, at low frequency, moving to a mass transfer process due to the corrosion products deposited on the metallic surface. Therefore, leading to impedance modulus values close to those achieved by AZ91 phosphate panels (Figure 5b).

3.2 Effect of the deposition of organosilane coatings on the AZ91 pre-treated surfaces

Surface modification is one efficient strategy to improve the corrosion resistance of Mg alloys. After the pre-treatment described above, a thin layer of silane (composed by TEOS and MTMS, hereafter called 3MT) was deposited by dip-coating onto the polished AZ91 disks. Characterization of the formed protecting film was conducted using SEM, XPS and EIS.

Bode plots recorded after 1h and 24 h of exposition to chloride solution, are displayed in the Figure 6. The pre-treatment with acetic acid had a harmful effect for the deposition of the 3MT coating, which was evidenced by the fact that the phase angle profile at high and medium frequencies are similar to that of AZ91 acetic specimens after 1h (Figure 6a). Nevertheless, in the coated 3MT alloy, the inductive points appeared at low frequencies, resulting in high impedance modulus values (10^3 to $10^{4.1}$ Ω cm^2). The same Bode profile was detected for AZ91 specimens polished and coated with 3MT films. Thus, for this system the electrochemical behavior is similar to that of bare alloy, suggesting that the metallic surface is partially covered by silica films. This is the reason for what the corrosion products were observed onto such surfaces, as was confirmed by XPS (discussed below).

On the other hand, Bode plots of AZ91 disks pre-treated with phosphate and hydrofluoric agents, and further coated with a 3MT layer, display two time constants after 1 hour of immersion in NaCl (Figure 6a). The first time constant (τ_1), which is observed at high frequency, has been associated to the capacitive response of the silica film, while the second time constant (τ_2) at medium frequency correspond to corrosion processes [23,31,49–51]. After 24 hours of samples immersion, the time constant at high frequency is only detected for the coated AZ91 phosphate samples (Figure 6b), which experience a slight reduction of their impedance modulus with increase immersion time (from $10^{4.7}$ to $10^{4.4}$ Ω cm^2, 1h and 24h, respectively). The Bode curve of 3MT-coated AZ91 hydrofluoric disk, immersed by 24 hours in the NaCl solution, shows a relaxation process exclusively at medium and low frequencies. This may be due to the non-homogenous silica film, which does not completely cover the cracks generated on the MgF_2 coating during the pre-treatment of metal surface with HF (*i.e.* aggressive agents quickly penetrate into the silica network and loss of the protective properties occurrs). EIS analyses suggest that the

pre-treatment with Na_3PO_4/NaOH is more efficient for the further obtaining of a homogenous and durable silica film onto the Mg alloy surface.

Figure 7 shows the morphology of silica films on Mg alloy submitted to different pre-treatments and, subsequently coated with the 3MT layer. In the Mg alloy polished with a grit and without pickling (Figure 7a), the horizontal marks from SiC mechanical grinding decrease with respect to the uncoated surface (Figure 1a). In spite of this, some agglomerates and micrometric cracks are observed (Figures 7b-c), explaining the penetration of the electrolyte towards the metal substrate after immersion in the NaCl solution. This is probably due to the brittleness and irregular adhesion of the film to the metal surface, as stated before [34,35,37]. The SEM micrographs are fully consistent with the EIS response, previously discussed.

Otherwise, the deposition of 3MT on the surface of AZ91 phosphate disks favors the deposition of homogenous and thick films (Figures 7d-e). Despite some microscopic cracks are observed above the surface (Figure 7f), they are superficial and small in comparison of those observed for the sanded surface samples. Moreover, no evidence of pitting or phosphate crystalline particles, like those observed by SEM before the silane deposition (Figure 2a), were detected in this case. These observations are also fully consistent with the EIS results (Figure 6) and XPS analyses (Figure 8, discussed below).

The good results achieved with basic solutions for the metal pre-treatment are in opposition with those obtained with the acidic solutions. The high roughness observed for the coated surface, after pre-treatment with acetic acid (Figures 7g-h), results on a heterogeneous morphology, with a highly porous layer. Moreover, the silane coating is not able to cover the AZ91 acetic rough surface, as evidenced in the high magnification SEM image (Figures 7i). A similar result was obtained for AZ91 hydrofluoric samples, in which the TEOS/MTMS films do not reach the enough thickness necessary to cover

all the fissures and pitting defects left by the MgF_2 conversion coating. Thus, Figures 7j-k indicate that several crevices were still present after the silane deposition. According to these results, the pre-treatment with the acid solutions should be avoided for the second step of this work, which consisted in the study of the influence of two different phosphonic acids on the improvement of the 3MT film forming properties.

XPS measurements were carried out to determine the concentration of main atoms present in the bilayer system, formed after the chemical pre-treatment and after the 3MT deposition on AZ91 alloy surface. Comparison of XPS survey spectra of AZ91 bare alloy and samples coated with silica films, previously submitted to three pre-treatments, are shown in the Figure 8. In general, the survey spectra contained O *1s*, C *1s* and Mg *2s* and Mg *2p* peaks, whereas Zn atoms were hardly seen. However, a very low content of Al atoms was found upon the metal surface when it was sputtered with Ar (belonging from its alloying composition) and when acetic acid was used as pickling agent (Table 2). Surface pickling with acetic acid will oxidize the metal surface, promoting the appearance of products like Al_2O_3. Even though Al_2O_3 agglomerates dissolve when the pH of the medium is low, residual compound will be detected by XPS. Therefore, Al atoms could belongs either from oxides materials upper metal surface or from the subsurface [51], due to the deficient 3M layer reported above.

Furthermore, after the silane deposition and curing, the content of carbon and silicon increases. AZ91 phosphate and hydrofluoric treated samples have similar composition in C, O and Si, whereas Mg, Al and Zn elements are not detected (Table 2). These results corroborate with the presence of a thick 3MT layer, fully covering the metal disk. Nevertheless, SEM analysis revealed that the 3MT films, over the MgF_2 passive layer formed in AZ91 hydrofluoric disks, are very brittle and exhibit crevices, allowing the liquid penetration and the subsequent metal corrosion. In order to investigate the efficacy

of the etching treatment, phosphorous and fluorine elements were also examined by high resolution XPS. A very low content of F *1s* was observed in all samples (Table 2), included those that were not treated with HF solution. Accordingly, we concluded that such small percentage comes from external contamination and is not a consequence of the chemical pre-treatment.

High resolution XPS spectra of C *1s*, O *1s*, Mg *2p*, Mg *2s* and Si *2p* are compared in Figures S1-S5. The Mg *2s* and Mg *2p* peaks (88 eV and 49.9 eV, respectively), which refers to the metallic atom; are well sharped in the disk without chemical pickling (Figure S1). By contrary, they become broad (peak between 48-52 eV) and with very low intensity, when covered with 3MT film (Figure S2), whereas the most important and intense peaks belong from silane material (C, O and Si atoms). In contrast, the Mg *2p* peak obtained for the AZ91 acetic sample (Figure S3) has been assigned to MgO oxide, since it appears at higher binding energy (50.6 eV) than the metallic atom. Samples with a thick 3MT layer had the same neighborhood linkages for Si *2p* orbital (103.2-103.4 eV), confirming the presence of well-defined Si–O–Si linkages in the silica network [51–53]. The O *1s* peak is clearly split in the pristine Mg alloy (Figure S1), which corresponds to C-O groups from carbonaceous contamination. On the other hand, the unique peak of O 1s obtained for the other samples, mainly corresponds to Si–O–Si linkages [56] (Figures S2-S5). These features are consistent with the silica network homogenously formed onto the metallic surface and reported previously [33,34].

In summary, the Na_3PO_4/NaOH pre-treatment offers the better and more durable protection, facilitating the sol-gel deposition of a uniform 3MT protective coating. Therefore, the pre-treatments with acetic acid and HF have been discarded for the study of phosphonic acid modification, which is aimed to evaluate the effect of a catalytic amount of phosphonic groups on the sol-gel film forming properties.

3.3 Effect of phosphonic acid addition in sol-gel films and AZ91 protection

In order to promote the formation of an adherent silane layer and, consequently, improve the corrosion protection of the metal surface, the effects of two phosphonic acids, were evaluated. Figure 9 displays the Bode plots recorded for AZ91 phosphate disks coated with 3MT (code: PhN3MT), 3MT and EDTPO (code: PhN3MT-E5), or 3MT and PhPA (code: PhN3MT-P5) after 1 and 72 hours of exposition on chloride-ion containing solution. The incorporation of phosphonic acids results in an increment of the phase angle at high frequency due to a modification in the relaxation process. This effect has been attributed to an increase of the film thickness and a reduction of the defects at the interface metal oxide-silane coating. In our case, both films (with and without phosphonic groups) actuate as barrier layers, since the electrolyte penetrates to the coating. However, the film without phosphonic groups has an extremely high porosity. Comparing the cross-section images of Figure S6 with Figures S7 and S8, it is evidenced that the film without phosphonic acid will lose the barrier property with time. For example, after 24 hours of immersion test, the phase angle of PhN3MT, PhN3MT-E5 and PhN3MT-Ph5 samples has changed to -56º, -72º and -71º, respectively, with the lower value for sample without phosphorous compounds. Furthermore, the beneficial effect on the Mg alloy corrosion resistance of phosphonic acids is also evidenced by the increment in the low-frequency impedance modulus |Z| (Figure 9) of PhN3MT-E5 and PhN3MT-Ph5, with respect to PhN3MT. The film thicknesses can be observed in the Figures S6-S8.

In order to understand the role played by the phosphonic acids, experimental data were fitted to an electrical equivalent circuit (EEC), consisting of two time constants (τ_1 and τ_2) in parallel: $R_s(R_1[CPE_1(R_2CPE_2)])$. The EEC results offer the lowest error with respect to experimental data. The following elements can be identified: R_s represents the

electrolyte resistance between the reference electrode and the working electrode; R_1 and CPE_1 correspond to the first time constant (τ_1), which comprises the silica network and the interfacial layer made of magnesium hydroxide/oxide layer and metal-siloxane bonds (*i.e.* these elements are related with the global barrier system and its electrical properties); R_2 and CPE_2 refer to the second time constant (τ_2) for the electrochemical reactions at metal surface [24,56] and correspond to the charge transfer resistance (R_{ct}) and double layer constant phase element (CPE_{dl}), respectively. The Bode plots with the fitted curves are included in the Figure 9.

The variation of R_1, which corresponds to the resistance of the bulk coating, against the immersion time is represented in Figure 10. As it was expected, R_1 decays after immersion in NaCl solution in all cases. Nevertheless, after 24 hours the R_1 value is 1.5 times higher for PhN3MT-E5 and PhN3MT-P5 than for PhN3MT. After 72 hours of immersion, the coating resistance determined for PhN3MT, PhN3MT-E5 and PhN3MT-P5 was R_1= 7.40, 19.1 and 17.8 kΩ cm^2, respectively (Figure 10a, Table S1). Nevertheless, the CPE_1 values, which are related to the water uptake of the coatings, increases with the immersion time (Figure 10b). Furthermore, PhN3MT-P5 and PhN3MT-E5 exhibited lower values than PhN3MT, indicating that the coatings of the former samples undergo moderate water absorption compared to the coating of the latter. For example, after 24 hours the CPE_1 was 0.80 and 0.78 µF cm^{-2} s^{n-1} for PhN3MT-E5 and PhN3MT-P5, respectively, while it was 4.75 µF cm^{-2} s^{n-1} for PhN3MT. It is worth noting that the silica network coating containing EDTPO, which offer multiple interactions with the Mg surface through four phosphonic acid groups (Scheme 1), exhibits the least pronounced water uptake variation. These features suggest that the phosphonic acid assists the silica network formation, improving the barrier system, which is fully consistent with previous investigations on aluminum substrates [35,36].

A second resistance response, R_2, appeared from the beginning of the assay due to the charge transfer process caused by the film porosity, which creates an easy pathway to water and chloride penetration. The R_2 values are much higher for PhN3MT-E5 than for PhN3MT and PhN3MT-P5, independently of the immersion time (Figure 10c). After 48 hours, the resistance of PhN3MT-E5, PhN3MT-P5 and PhN3MT was R_2= 51.2, 24.9 and 4.3 kΩ cm^2, respectively. The Mg alloy coated with the EDTPO-containing sol-gel film showed the highest R_2 and the lowest CPE_2 values. These results indicate that the number of active phosphonic groups in the sol-gel solution is important for both the film forming properties (after hydrolysis and condensation) and the corrosion protection of the metal surface.

As depicted in the Scheme 1, the main difference between the EDTPO and PhPA is the number of phosphonic acid groups (*i.e.* four and one, respectively). In previous works [34,36], we proposed a model for the chemical interaction among phosphonic groups, silica network and aluminum substrate, which could occur through mono or bidentate coordination with the metallic surface. In the present study, we also confirm the good performance of PhN3MT-E5 system due to its higher number of phosphonic acid bonds interacting with the silica network and the metal surface, than PhN3MT-P5, with only one phosphonic acid group.

SEM micrographs showed in the Figure 11 correspond to the topographic and cross-section morphologies of 3MT-phosphonic and PhN3MT-E5 systems. As can be seen, in the Figures 11a-b, the 3MT film is porous, thin, and has some crevices and holes (circles inserted). By contrary, the deposition of silica onto the Mg alloy surface, after the addition of a catalytic amount of EDTPO molecules, gives rise to a completely homogeneous film, thick, and free of defects (Figures 11c-d). All the defects caused by the Na_3PO_4/NaOH pre-treatment (Figures 2a-d) were completely covered by the organophosphonate-silane

coating. Thus, this uniform layer is able to prevent the metal from the electrolyte penetration, acting as a barrier layer. In summary, both impedance analyses and SEM micrographs proved that the PhN3MT-E5 coating is able to protect the Mg alloy for more than 72 hours in 0.05 M NaCl solution, providing better barrier properties than the 3MT film without phosphoric groups.

4. Conclusions

Significant differences in both the electrochemical behavior and the morphology of metal oxides/hydroxides have been obtained by varying the chemical pre-treatment of the AZ91 alloy. SEM, XPS and electrochemical assays have demonstrated that the pre-treatment with Na_3PO_4/NaOH provides a good and stable passivated hydroxide layer, facilitating the further deposition of silane coating. Thus, the alkaline pre-treatment of the AZ91 alloy surface exhibits advantages with respect to acid pickling (either with acetic acid or with hydrofluoric acid). On the other hand, EIS measurements have indicated the distinctive effects of the catalytic addition of EDTPO or PhPA molecules in the sol-gel solution. EDTPO propitiates a fully covered metal surface and the elimination of the defects produced by the alkaline pre-treatment, leading to an enhanced barrier protection for the metal substrate. Overall, the best hybrid sol-gel film for the protection of the AZ91 Mg alloy against corrosive NaCl solutions is that composed by TEOS and MTMS silane comonomers and EDTPO molecules. This improved performance of EDTPO containing films have been attributed to the multiple bonds formed among silica network, phosphonic groups and magnesium-oxide/hydroxide inner layer.

Acknowledgements

This work was supported by CNPq (nº 306818/2014, Brazil), MINECO (MAT2015-69367-R, Spain) and the Agència de Gestió d'Ajuts Universitaris i de Recerca (2017SGR359) funds. Support for the research by C. A. was received through the prize "ICREA Academia 2015" for excellence in research, funded by the Generalitat de Catalunya (Catalonia-Spain). Authors acknowledge Dr. T. Trifonov for his help with the FIB-SEM analyses, and also Dr. M. Dominguez and L. Calvo, for the XPS measurements.

References

[1] Clow B.B., Advanced Materials & Processes, ASM Int. (1996) 33.
[2] Polmear I.J., Light Alloys: Metallurgy of the Light Metals, 2nd ed., Edward Arnold, London - Melbourne, 1989.
[3] T. Ishizaki, S. Chiba, H. Suzuki, In Situ Formation of Anticorrosive Mg-Al Layered Double Hydroxide-Containing Magnesium Hydroxide Film on Magnesium Alloy by Steam Coating, Ecs Electrochem. Lett. 2 (2013) C15–C17. doi:10.1149/2.006305eel.
[4] G. Williams, H.A.L. Dafydd, R. Grace, The localised corrosion of Mg alloy AZ31 in chloride containingelectrolyte studied by a scanning vibrating electrode technique, Electrochim. Acta. 109 (2013) 489–501. doi:10.1016/j.electacta.2013.07.134.
[5] G.L. Song, Z. Xu, The surface, microstructure and corrosion of magnesium alloy AZ31 sheet, Electrochim. Acta. 55 (2010) 4148–4161. doi:10.1016/j.electacta.2010.02.068.
[6] A. Zomorodian, C. Santos, M.J. Carmezim, T.M. e Silva, J.C.S. Fernandes, M.F. Montemor, "In-vitro" corrosion behaviour of the magnesium alloy with Al and Zn (AZ31) protected with a biodegradable polycaprolactone coating loaded with hydroxyapatite and cephalexin, Electrochim. Acta. 179 (2015) 431–440. doi:10.1016/J.ELECTACTA.2015.04.013.
[7] A. Zomorodian, I.A. Ribeiro, J.C.S. Fernandes, A.C. Matos, C. Santos, A.F. Bettencourt, M.F. Montemor, Biopolymeric coatings for delivery of antibiotic and controlled degradation of bioresorbable Mg AZ31 alloys, Int. J. Polym. Mater. Polym. Biomater. 66 (2017) 533–543. doi:10.1080/00914037.2016.1252347.
[8] G.L. Song, A. Atrens, Corrosion Mechanisms of Magnesium Alloys, Adv. Eng. Mater. 1 (1999) 11–33. doi:10.1002/(SICI)1527-2648(199909)1:1<11::AID-ADEM11>3.0.CO;2-N.
[9] A. Pardo, M.C. Merino, A.E. Coy, F. Viejo, R. Arrabal, S. Feli??, Influence of microstructure and composition on the corrosion behaviour of Mg/Al alloys in chloride media, Electrochim. Acta. 53 (2008) 7890–7902. doi:10.1016/j.electacta.2008.06.001.
[10] B.L. Mordike, T. Ebert, Magnesium - Properties - applications - potential, Mater. Sci. Eng. a-Structural Mater. Prop. Microstruct. Process. 302 (2001) 37–45. doi:10.1016/s0921-5093(00)01351-4.

[11] R. Ambat, N.N. Aung, W. Zhou, Evaluation of microstructural effects on corrosion behaviour of AZ91D magnesium alloy, Corros. Sci. 42 (2000) 1433–1455. doi:10.1016/S0010-938X(99)00143-2.
[12] G. Song, A. Atrens, X. Wu, B. Zhang, Corrosion behaviour of AZ21, AZ501 and AZ91 in sodium chloride, Corros. Sci. 40 (1998) 1769–1791.
[13] A. Pardo, M.C. Merino, A.E. Coy, R. Arrabal, F. Viejo, E. Matykina, Corrosion behaviour of magnesium/aluminium alloys in 3.5 wt.% NaCl, Corros. Sci. 50 (2008) 823–834. doi:10.1016/j.corsci.2007.11.005.
[14] K. Brunelli, M. Dabalà, I. Calliari, M. Magrini, Effect of HCl pre-treatment on corrosion resistance of cerium-based conversion coatings on magnesium and magnesium alloys, Corros. Sci. 47 (2005) 989–1000. doi:10.1016/j.corsci.2004.06.016.
[15] H.H. Elsentriecy, K. Azumi, H. Konno, Effect of surface pretreatment by acid pickling on the density of stannate conversion coatings formed on AZ91 D magnesium alloy, Surf. Coatings Technol. 202 (2007) 532–537. doi:10.1016/j.surfcoat.2007.06.033.
[16] A.M. Lafront, W. Zhang, S. Jin, R. Tremblay, D. Dubé, E. Ghali, Pitting corrosion of AZ91D and AJ62x magnesium alloys in alkaline chloride medium using electrochemical techniques, Electrochim. Acta. 51 (2005) 489–501. doi:10.1016/j.electacta.2005.05.013.
[17] T. Zhang, Y. Shao, G. Meng, F. Wang, Electrochemical noise analysis of the corrosion of AZ91D magnesium alloy in alkaline chloride solution, Electrochim. Acta. 53 (2007) 561–568. doi:10.1016/j.electacta.2007.07.014.
[18] H.Y. Yang, X.B. Chen, X.W. Guo, G.H. Wu, W.J. Ding, N. Birbilis, Coating pretreatment for Mg alloy AZ91D, Appl. Surf. Sci. 258 (2012) 5472–5481. doi:10.1016/j.apsusc.2012.02.044.
[19] N.I.Z. Abidin, A. Da Forno, M. Bestetti, D. Martin, A. Beer, A. Atrens, Evaluation of coatings for Mg alloys for biomedical applications, Adv. Eng. Mater. 17 (2015) 58–67. doi:10.1002/adem.201300516.
[20] Y. Xin, C. Liu, X. Zhang, G. Tang, X. Tian, P.K. Chu, Corrosion behavior of biomedical AZ91 magnesium alloy in simulated body fluids, J. Mater. Res. 22 (2007) 2004–2011. doi:10.1557/jmr.2007.0233.
[21] R.-C. Zeng, W.-C. Qi, F. Zhang, S.-Q. Li, In vitro corrosion of pure magnesium and AZ91 alloy—the influence of thin electrolyte layer thickness, Regen. Biomater. 3 (2016) 49–56. doi:10.1093/rb/rbv028.
[22] C. Ke, Y. Wu, Y. Qiu, J. Duan, N. Birbilis, X.B. Chen, Influence of surface chemistry on the formation of crystalline hydroxide coatings on Mg alloys in liquid water and steam systems, Corros. Sci. 113 (2016) 145–159. doi:10.1016/j.corsci.2016.10.017.
[23] F. Brusciotti, D. V. Snihirova, H. Xue, M.F. Montemor, S. V. Lamaka, M.G.S. Ferreira, Hybrid epoxy-silane coatings for improved corrosion protection of Mg alloy, Corros. Sci. 67 (2013) 82–90. doi:10.1016/j.corsci.2012.10.013.
[24] A. Zomorodian, M.P. Garcia, T. Moura E Silva, J.C.S. Fernandes, M.H. Fernandes, M.F. Montemor, Corrosion resistance of a composite polymeric coating applied on biodegradable AZ31 magnesium alloy, Acta Biomater. 9 (2013) 8660–8670. doi:10.1016/j.actbio.2013.02.036.
[25] F. Zhang, Z.-G. Liu, R.-C. Zeng, S.-Q. Li, H.-Z. Cui, L. Song, E.-H. Han, Corrosion resistance of Mg–Al-LDH coating on magnesium alloy AZ31, Surf. Coatings Technol. 258 (2014) 1152–1158.
[26] F. Brusciotti, D. V Snihirova, H. Xue, M.F. Montemor, S. V Lamaka, M.G.S.

Ferreira, Hybrid epoxy-silane coatings for improved corrosion protection of Mg alloy, Corros. Sci. 67 (2013) 82–90. doi:10.1016/j.corsci.2012.10.013.
[27] R.N. Peres, E.S.F. Cardoso, M.F. Montemor, H.G. de Melo, A.V. Benedetti, P.H. Suegama, Influence of the addition of SiO2 nanoparticles to a hybrid coating applied on an AZ31 alloy for early corrosion protection, Surf. Coatings Technol. 303 (2016) 372–384. doi:10.1016/J.SURFCOAT.2015.12.049.
[28] L.C. Córdoba, M.F. Montemor, T. Coradin, Silane/TiO 2 coating to control the corrosion rate of magnesium alloys in simulated body fluid, Corros. Sci. 104 (2016) 152–161. doi:10.1016/j.corsci.2015.12.006.
[29] S.H. Adsul, T. Siva, S. Sathiyanarayanan, S.H. Sonawane, R. Subasri, Self-healing ability of nanoclay-based hybrid sol-gel coatings on magnesium alloy AZ91D, Surf. Coatings Technol. 309 (2017) 609–620. doi:10.1016/j.surfcoat.2016.12.018.
[30] D.K. Ivanou, K.A. Yasakau, S. Kallip, A.D. Lisenkov, M. Starykevich, S. V. Lamaka, M.G.S. Ferreira, M.L. Zheludkevich, Active corrosion protection coating for a ZE41 magnesium alloy created by combining PEO and sol–gel techniques, RSC Adv. 6 (2016) 12553–12560. doi:10.1039/C5RA22639B.
[31] A. Castellanos, A. Altube, J.M. Vega, E. García-Lecina, J.A. Díez, H.J. Grande, Effect of different post-treatments on the corrosion resistance and tribological properties of AZ91D magnesium alloy coated PEO, Surf. Coatings Technol. 278 (2015) 99–107. doi:10.1016/j.surfcoat.2015.07.017.
[32] J.Y. Hu, Q. Li, X.K. Zhong, F. Luo, Fluoride treatment and sol film composite technology for AZ91D magnesium alloy, Trans. IMF. 88 (2010) 41–46. doi:10.1179/174591910X12596809947256.
[33] V. Dalmoro, J.H.Z. dos Santos, E. Armelin, C. Alemán, D. Schermann Azambuja, Phosphonic acid/silica-based films: A potential treatment for corrosion protection, Corros. Sci. 60 (2012) 173–180. doi:10.1016/j.corsci.2012.03.040.
[34] V. Dalmoro, J.H.Z. dos Santos, E. Armelin, C. Alemán, D.S. Azambuja, A synergistic combination of tetraethylorthosilicate and multiphosphonic acid offers excellent corrosion protection to AA1100 aluminum alloy, Appl. Surf. Sci. 273 (2013) 758–768. doi:10.1016/j.apsusc.2013.02.131.
[35] V. Dalmoro, J.H.Z. Dos Santos, I.M. Baibich, I.S. Butler, E. Armelin, C. Alemán, D.S. Azambuja, Improving the corrosion performance of hybrid sol-gel matrix by modification with phosphonic acid, Prog. Org. Coatings. 80 (2015) 49–58. doi:10.1016/j.porgcoat.2014.11.018.
[36] J. Torras, D.S. Azambuja, J.M. Wolf, C. Alemán, E. Armelin, How organophosphonic acid promotes silane deposition onto aluminum surface: A detailed investigation on adsorption mechanism, J. Phys. Chem. C. 118 (2014) 17724−17736. doi:10.1021/jp5046707.
[37] V. Dalmoro, C. Alemán, C.A. Ferreira, J.H.Z. Dos Santos, D.S. Azambuja, E. Armelin, The influence of organophosphonic acid and conducting polymer on the adhesion and protection of epoxy coating on aluminium alloy, Prog. Org. Coatings. 88 (2015) 181–190. doi:10.1016/j.porgcoat.2015.07.004.
[38] J.I. Iribarren-Mateos, I. Buj-Corral, J. Vivancos-Calvet, C. Alemán, J.I. Iribarren, E. Armelin, Silane and epoxy coatings: A bilayer system to protect AA2024 alloy, Prog. Org. Coatings. 81 (2015) 47–57. doi:10.1016/j.porgcoat.2014.12.014.
[39] Z.-H. Xie, F. Chen, S.-R. Xiang, J.-L. Zhou, Z.-W. Song, G. Yu, Studies of Several Pickling and Activation Processes for Electroless Ni-P Plating on AZ31

Magnesium Alloy, J. Electrochem. Soc. 162 (2014) D115–D123. doi:10.1149/2.0601503jes.
[40] T.F. Da Conceicao, N. Scharnagl, C. Blawert, W. Dietzel, K.U. Kainer, Surface modification of magnesium alloy AZ31 by hydrofluoric acid treatment and its effect on the corrosion behaviour, Thin Solid Films. 518 (2010) 5209–5218. doi:10.1016/j.tsf.2010.04.114.
[41] S.T. Jiang, J. Zhang, S.Z. Shun, M.F. Chen, The formation of FHA coating on biodegradable Mg-Zn-Zr alloy using a two-step chemical treatment method, Appl. Surf. Sci. 388 (2016) 424–430. doi:10.1016/j.apsusc.2015.12.087.
[42] J.D. Verink, Simplified Procedure for Constructing Pourbaix Diagrams, in: Uhlig's Corros. Handb. Third Ed., 2011: pp. 93–101. doi:10.1002/9780470872864.ch7.
[43] Y. Zhu, G. Yu, B. Hu, X. Lei, H. Yi, J. Zhang, Electrochemical behaviors of the magnesium alloy substrates in various pretreatment solutions, Appl. Surf. Sci. 256 (2010) 2988–2994. doi:10.1016/j.apsusc.2009.11.062.
[44] T. Yan, L. Tan, B. Zhang, K. Yang, Preparation and characterization of fluoride conversion coating on biodegradable AZ31B magnesium alloy, J. Optoelectron. Adv. Mater. 16 (2014) 562–567. doi:10.1016/j.jmst.2013.12.015.
[45] A. Zomorodian, F. Brusciotti, A. Fernandes, M.J. Carmezim, T. Moura e Silva, J.C.S. Fernandes, M.F. Montemor, Anti-corrosion performance of a new silane coating for corrosion protection of AZ31 magnesium alloy in Hank's solution, Surf. Coatings Technol. 206 (2012) 4368–4375. doi:10.1016/j.surfcoat.2012.04.061.
[46] S.E. Frers, M.M. Stefenel, C. Mayer, T. Chierchie, AC-Impedance measurements on aluminium in chloride containing solutions and below the pitting potential, J. Appl. Electrochem. 20 (1990) 996–999. doi:10.1007/BF01019578.
[47] S. Mathieu, C. Rapin, J. Steinmetz, P. Steinmetz, A corrosion study of the main constituent phases of AZ91 magnesium alloys, Corros. Sci. 45 (2003) 2741–2755. doi:10.1016/S0010-938X(03)00109-4.
[48] G. Baril, N. Pébère, Corrosion of pure magnesium in aerated and deaerated sodium sulphate solutions, Corros. Sci. 43 (2001) 471–484. doi:10.1016/S0010-938X(00)00095-0.
[49] S.V. Lamaka, G. Knörnschild, D.V. Snihirova, M.G. Taryba, M.L. Zheludkevich, M.G.S. Ferreira, Complex anticorrosion coating for ZK30 magnesium alloy, Electrochim. Acta. 55 (2009) 131–141. doi:10.1016/j.electacta.2009.08.018.
[50] I.A. Kartsonakis, A.C. Balaskas, E.P. Koumoulos, C.A. Charitidis, G. Kordas, Evaluation of corrosion resistance of magnesium alloy ZK10 coated with hybrid organic-inorganic film including containers, Corros. Sci. 65 (2012) 481–493. doi:10.1016/j.corsci.2012.08.052.
[51] C. Liu, Y. Xin, X. Tian, P.K. Chu, Corrosion behavior of AZ91 magnesium alloy treated by plasma immersion ion implantation and deposition in artificial physiological fluids, Thin Solid Films. 516 (2007) 422–427. doi:10.1016/j.tsf.2007.05.048.
[52] M.. Capel-Sanchez, L. Barrio, J.. Campos-Martin, J.L.. Fierro, Silylation and surface properties of chemically grafted hydrophobic silica, J. Colloid Interface Sci. 277 (2004) 146–153. doi:10.1016/j.jcis.2004.04.055.
[53] X. Lu, Y. Zuo, X. Zhao, Y. Tang, The improved performance of a Mg-rich epoxy coating on AZ91D magnesium alloy by silane pretreatment, Corros. Sci. 60 (2012) 165–172. doi:10.1016/j.corsci.2012.03.041.
[54] N.I. Zainal Abidin, D. Martin, A. Atrens, Corrosion of high purity Mg, AZ91,

ZE41 and Mg2Zn0.2Mn in Hank's solution at room temperature, Corros. Sci. 53 (2011) 862–872. doi:10.1016/j.corsci.2010.10.008.
[55] N.I. Zainal Abidin, B. Rolfe, H. Owen, J. Malisano, D. Martin, J. Hofstetter, P.J. Uggowitzer, A. Atrens, The in vivo and in vitro corrosion of high-purity magnesium and magnesium alloys WZ21 and AZ91, Corros. Sci. 75 (2013) 354–366. doi:10.1016/j.corsci.2013.06.019.
[56] Y.Y. Yue, Z.X. Liu, T.T. Wan, P.C. Wang, Effect of phosphate-silane pretreatment on the corrosion resistance and adhesive-bonded performance of the AZ31 magnesium alloys, Prog. Org. Coatings. 76 (2013) 835–843. doi:10.1016/j.porgcoat.2013.01.010.

Table 1. Description of the phosphonic acid concentrations in the silane sol-gel solutions and codes used for the identification of films deposited on Mg alloy surface.

Pre-treatment	**Sol-gel film**	**Phosphonic acid**	**Phosphonic acid concentration (mol L^{-1})**	**Label**
Sanded with SiC abrasive paper	TEOS/MTMS	-	-	3MT
Hydrofluoric acid	TEOS/MTMS	-	-	HF3MT
Acetic acid	TEOS/MTMS	-	-	Ac3MT
Phosphate/NaOH	TEOS/MTMS	-	-	PhN3MT
Phosphate/NaOH	TEOS/MTMS	EDTPO	3.75×10^{-5}	PhN3MT-E5
Phosphate/NaOH	TEOS/MTMS	PhPA	15.0×10^{-5}	PhN3MT-P5

Table 2. Atomic concentration (%) determined by XPS analyses for samples studied in this work.

Sample	**Mg *2p***	**Al *2p***	**Zn *2p***	**C *1s***	**O *1s***	**Si *2p***	**P *2p***	**F *1s***
AZ91 disk[a)]	30.1	5.1	0.0	8.5	56.3	0.0	0.0	0.0
AZ91 sanded + 3MT coating	0.0	0.0	0.0	34.5	40.9	23.5	0.0	1.1
AZ91 acetic + 3MT coating	6.7	2.9	0.1	23.2	49.4	17.5	0.0	0.3
AZ91 phosphate + 3MT coating	0.0	0.0	0.0	24.6	47.4	27.6	0.0	0.4
AZ91 hydrofluoric + 3MT coating	0.0	0.0	0.0	27.9	45.8	26.0	0.0	0.4

[a)] Data obtained after 2 min of *in situ* sputtering in the XPS equipment.

Captions of Figures

Figure 1. (a-d) SEM micrographs of AZ91 Mg alloy mechanically sanded with SiC sand paper; (e) EDX obtained for different surface zones, which evidence high atomic percentage of Mg and low percentage of main alloying elements (Al and Zn).

Figure 2. AZ91 phosphate samples: (a-d) SEM micrographs of AZ91 Mg alloy surface mechanically sanded and treated with a Na_3PO_4/NaOH solution; (e) EDX spectra of different surface zones, which evidence a high atomic percentage of Mg, Al and oxygen elements, especially for the Spectrum 1, where the crystalline particles observed in the image d) has been analyzed. Phosphorous atoms were also detected (Spectrum 3), in low proportion respect to the main alloying atoms, from isolated solid particles upper the metal treated surface (image d).

Figure 3. AZ91 acetic samples: (a-d) SEM micrographs of AZ91 Mg alloy surface mechanically sanded and treated with acetic acid solution; (e) EDX analyses of different surface zones, which evidence a great amount of metal oxides or hydroxides from Mg, Al and Zn chemical combinations.

Figure 4. AZ91 hydrofluoric samples: (a-d) SEM micrographs of AZ91 Mg alloy surface mechanically sanded and pre-treated with HF solution. Different magnifications show the particles, agglomerates and thick layer formed after the pre-treatment with this acid solution. (e) EDX analyses of different surface zones, which evidence the high atomic concentration of fluorine atoms, probably due to the formation of MgF_2 layer after pickling treatment.

Figure 5. Bode plots of AZ91 disks polished with sand paper and submitted to pre-treatments with Na_3PO_4/NaOH, acetic acid and HF solutions, after (a) 1 hour and (b) 48 hours of immersion in 0.05 mol L^{-1} NaCl electrolyte solution.

Figure 6. Bode plots of the following samples: AZ91 Mg mechanically polished and coated with the sol-gel 3MT film (code: 3MT); AZ91 polished, pre-treated with acetic acid, and coated with the sol-gel 3MT film (code: Ac3MT); AZ91 polished, pre-treated with Na_3PO_4/NaOH, and coated with the sol-gel 3MT film (code: PhN3MT); and AZ91 polished, pre-treated with HF, and coated with the sol-gel 3MT film (code: HF3MT); after (a) 1 hour and (b) 24 hours of immersion in 0.05 mol L^{-1} NaCl electrolyte solution.

Figure 7. SEM micrographs of: (a,b,c) AZ91 Mg mechanically polished and coated with 3MT (3MT); (d,e,f) AZ91 Mg polished, pre-treated with Na_3PO_4/NaOH, and coated with 3MT (PhN3MT); (g,h,i) AZ91 polished, pre-treated with acetic acid, and coated with 3MT (Ac3MT); and, (j,k,l) AZ91 polished, pre-treated with HF, and coated with 3MT (HF3MT).

Figure 8. XPS survey spectra of 3MT, Ac3MT, PhN3MT and HF3MT coatings (samples' codes described in the Figure 7) and AZ91 bare surface, without any mechanical or chemical pre-treatments. The AZ91 sample was sputtered with argon for 2 min, before analysis.

Figure 9. Bode plots of AZ91 phosphate coated with 3MT (code: PhN3MT), 3MT and EDTPO (code: PhN3MT-E5), or 3MT and PhPA (code: PhN3MT-P5) after (a) 1 h and (b) 72 h of immersion in 0.05 mol L^{-1} NaCl electrolyte solution. Lines represent the EEC fitting curves.

Figure 10. Variation of the resistances and capacitances with the immersion time obtained from the EEC fitted for AZ91 phosphate samples coated with the sol-gel films without (PhN3MT) or with (PhN3MT-E5 and PhN3MT-P5) phosphonic acid.

Figure 11. (a) Surface topography of 3MT silane coating, after the treatment of AZ91 metal surface with phosphate/NaOH solution. The circles inset indicate the film crevices observed. (b) Cross-section of the 3MT transversal film, evidencing the presence of pores

inside the silica network and some inclusions due to the alkaline treatment, at the metal-silane interface. (c) Surface topography of PhN3MT-E5 coating, after the treatment of AZ91 metal surface with phosphate/NaOH solution. (d) Cross-section of PhN3MT-E5 transversal film, evidencing a well-adhered and homogenous organophosphonic-silane coating.

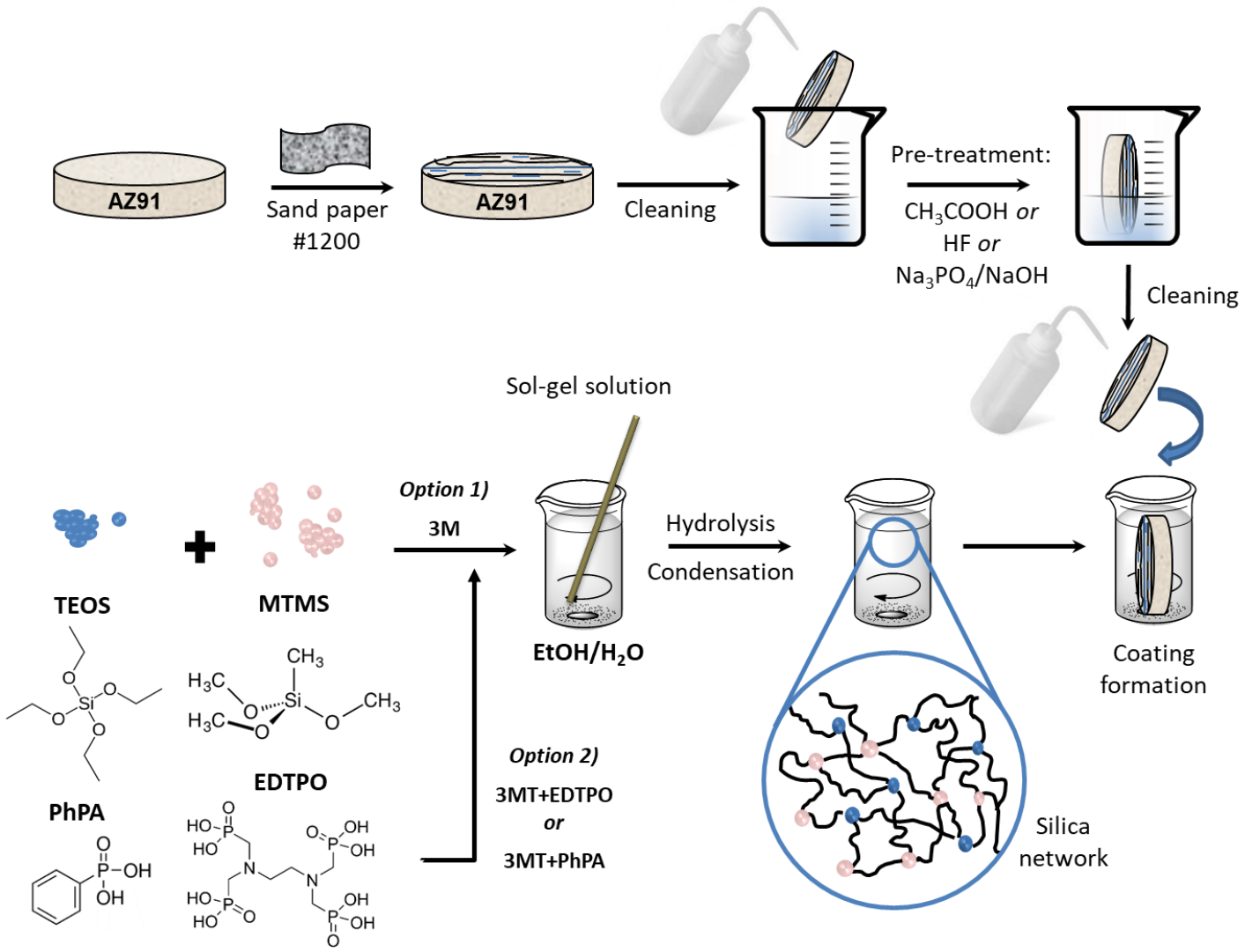

Scheme 1 Schematic representation of metal surface pre-treatments and organophosphonic-silane sol-gel deposition.

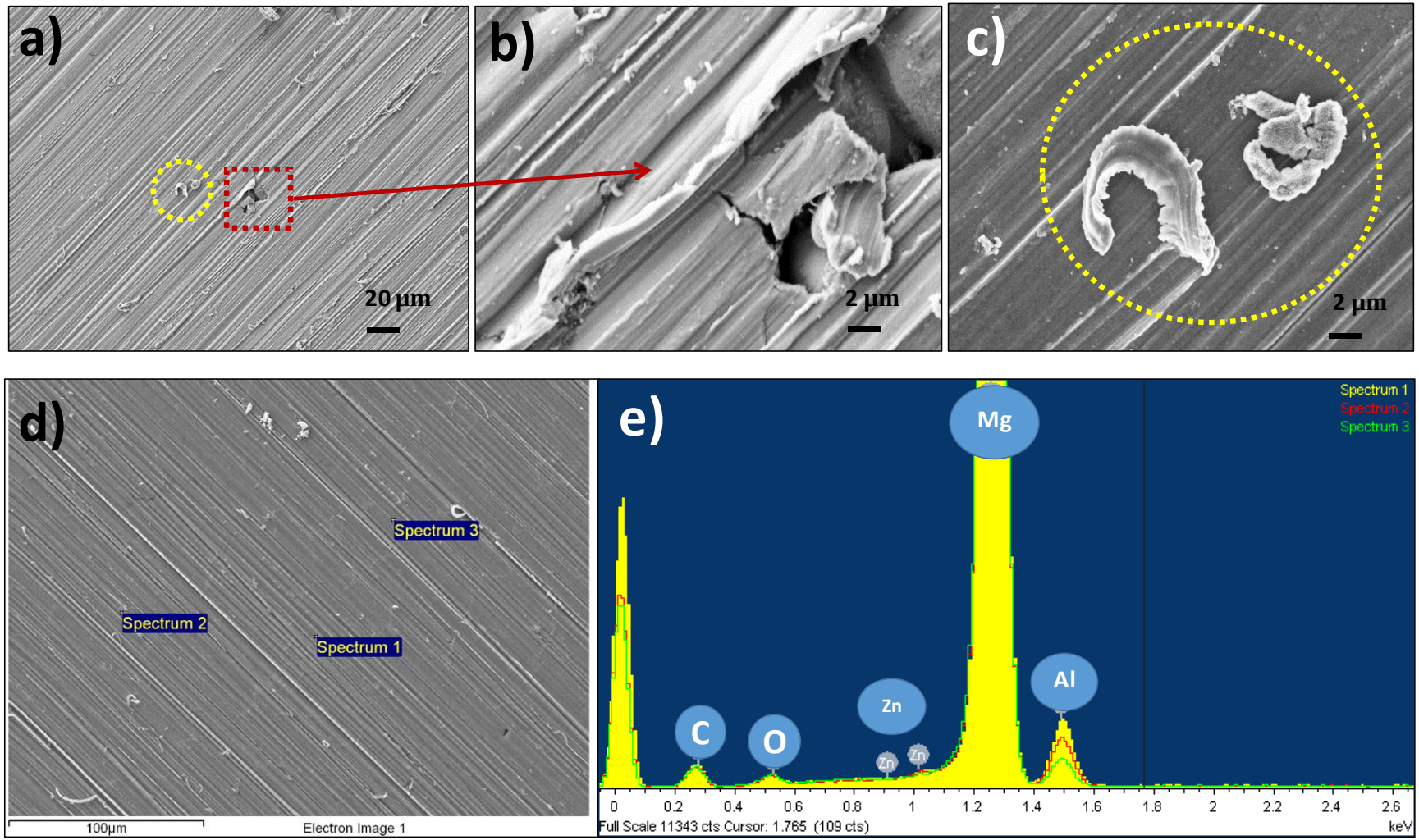
a)
20 µm
b)
2 µm
c)
2 µm
d)
Spectrum 3
Spectrum 2
Spectrum 1
100µm
Electron Image 1
e)
Spectrum 1
Spectrum 2
Spectrum 3
Mg
Al
Zn
C
O
Zn
Zn
0
0.2
0.4
0.6
0.8
1
1.2
1.4
1.6
1.8
2
2.2
2.4
2.6
Full Scale 11343 cts Cursor: 1.765 (109 cts)
keV

Figure 1

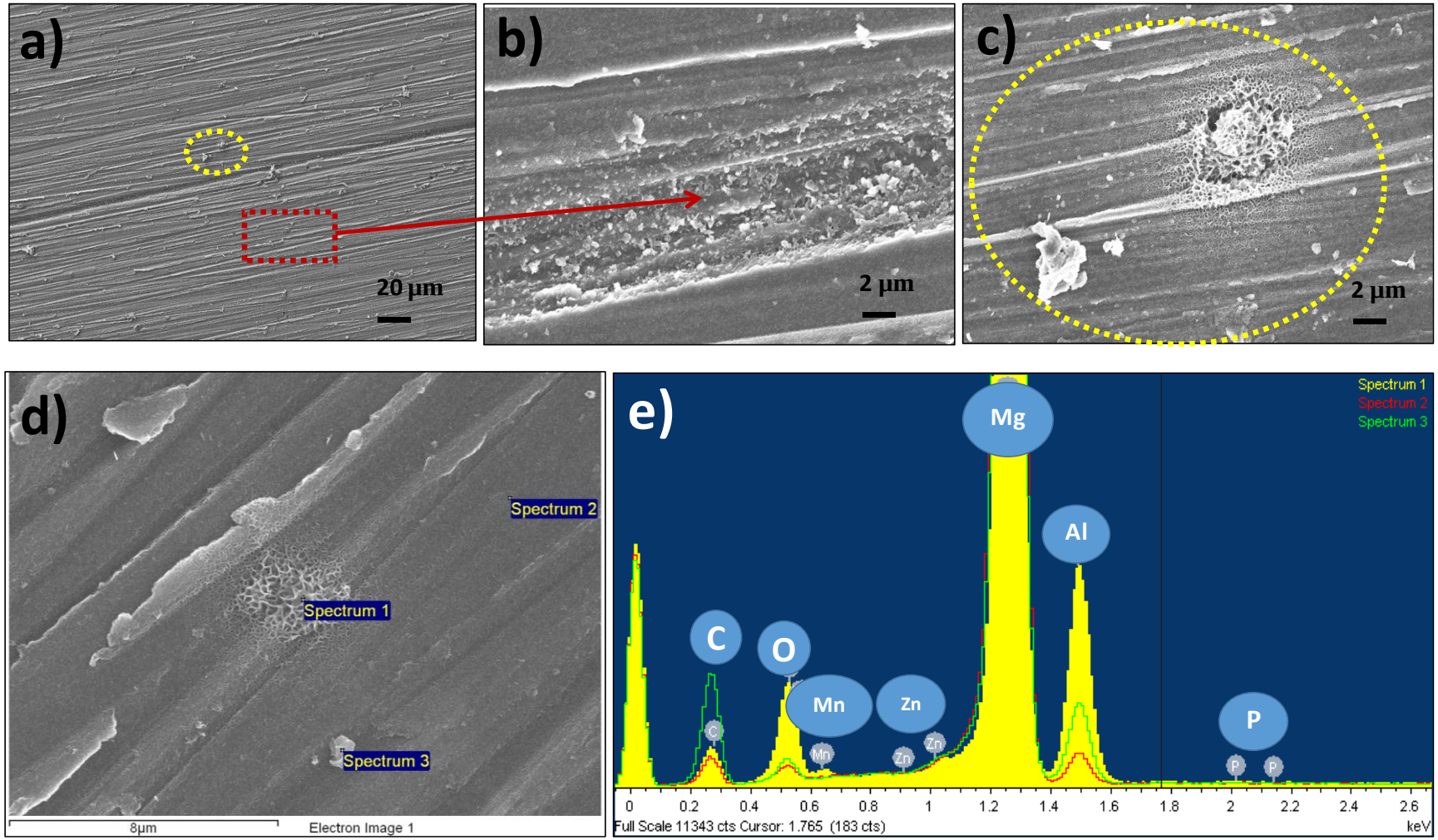
a)
20 µm
b)
2 µm
c)
2 µm
d)
Spectrum 2
Spectrum 1
Spectrum 3
8µm
Electron Image 1
e)
Spectrum 1
Spectrum 2
Spectrum 3
Mg
Al
C
O
Mn
Zn
P
0
0.2
0.4
0.6
0.8
1
1.2
1.4
1.6
1.8
2
2.2
2.4
2.6
Full Scale 11343 cts Cursor: 1.765 (183 cts)
keV

Figure 2

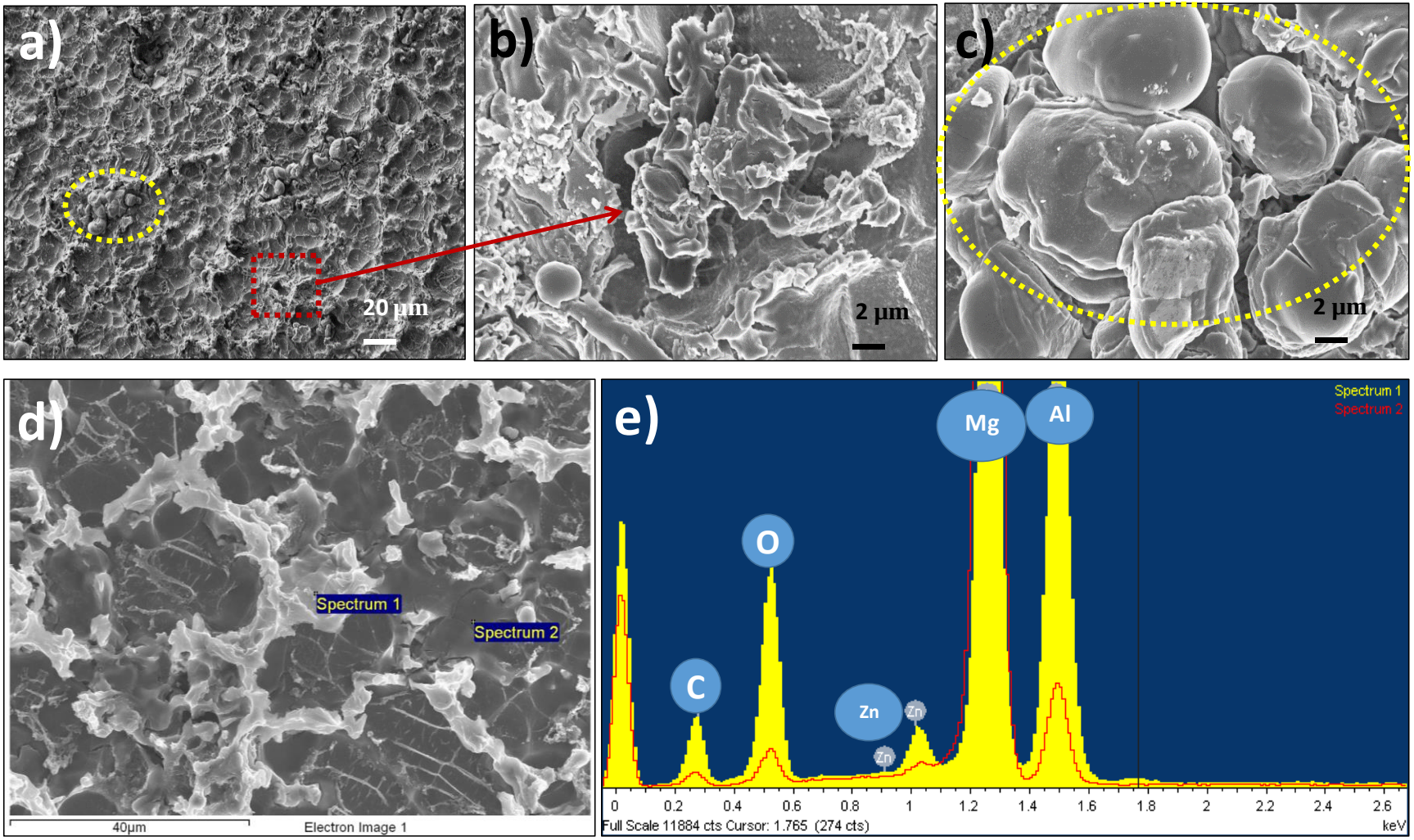
a)
20 µm
b)
2 µm
c)
2 µm
d)
Spectrum 1
Spectrum 2
40µm
Electron Image 1
e)
Spectrum 1
Spectrum 2
Mg
Al
O
C
Zn
Zn
Zn
0
0.2
0.4
0.6
0.8
1
1.2
1.4
1.6
1.8
2
2.2
2.4
2.6
Full Scale 11884 cts Cursor: 1.765 (274 cts)
keV

Figure 3

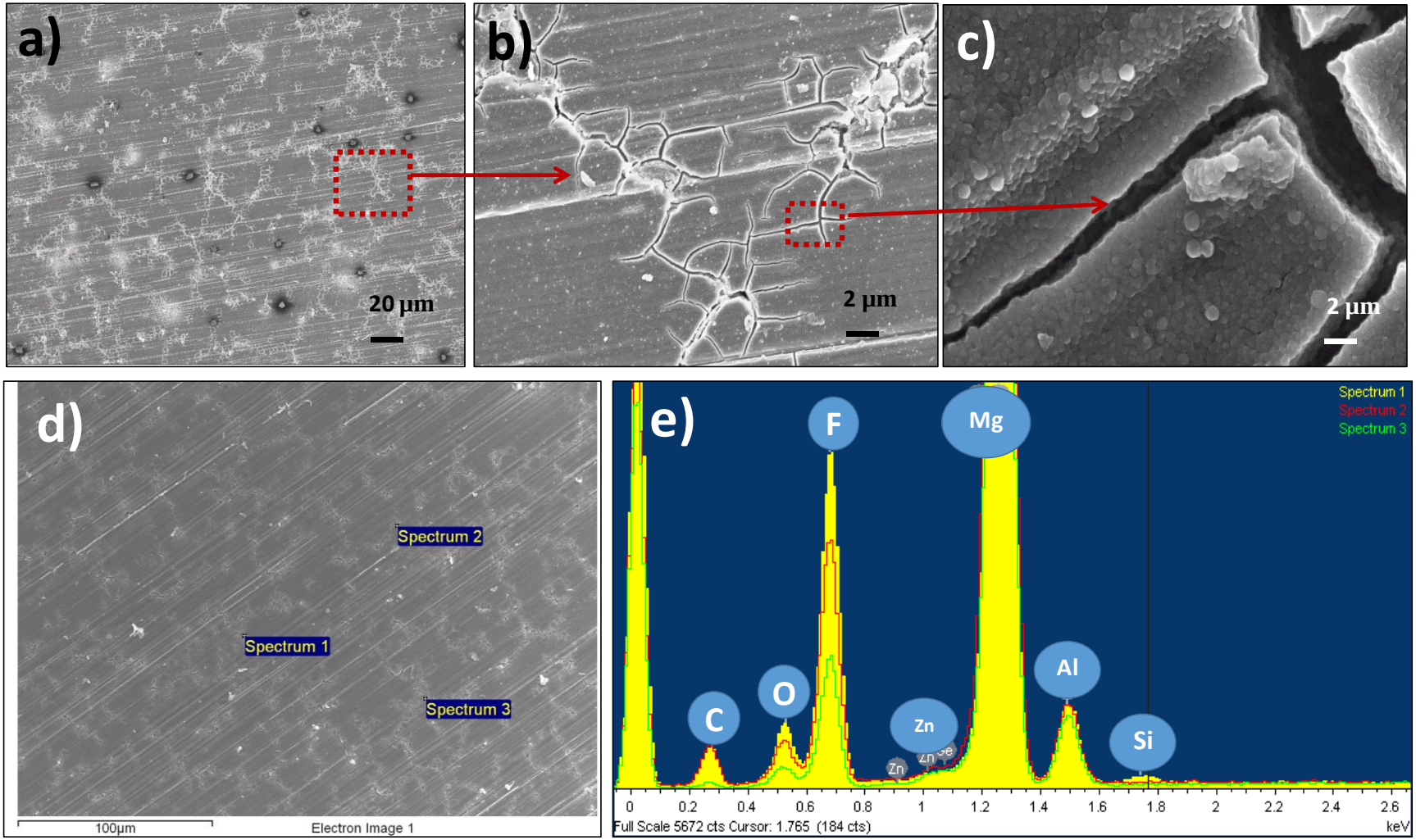
a)
20 µm
b)
2 µm
c)
2 µm
d)
Spectrum 2
Spectrum 1
Spectrum 3
100µm
Electron Image 1
e)
F
Mg
C
O
Zn
Al
Si
Spectrum 1
Spectrum 2
Spectrum 3
0 0.2 0.4 0.6 0.8 1 1.2 1.4 1.6 1.8 2 2.2 2.4 2.6
Full Scale 5672 cts Cursor: 1.765 (184 cts)
keV

Figure 4

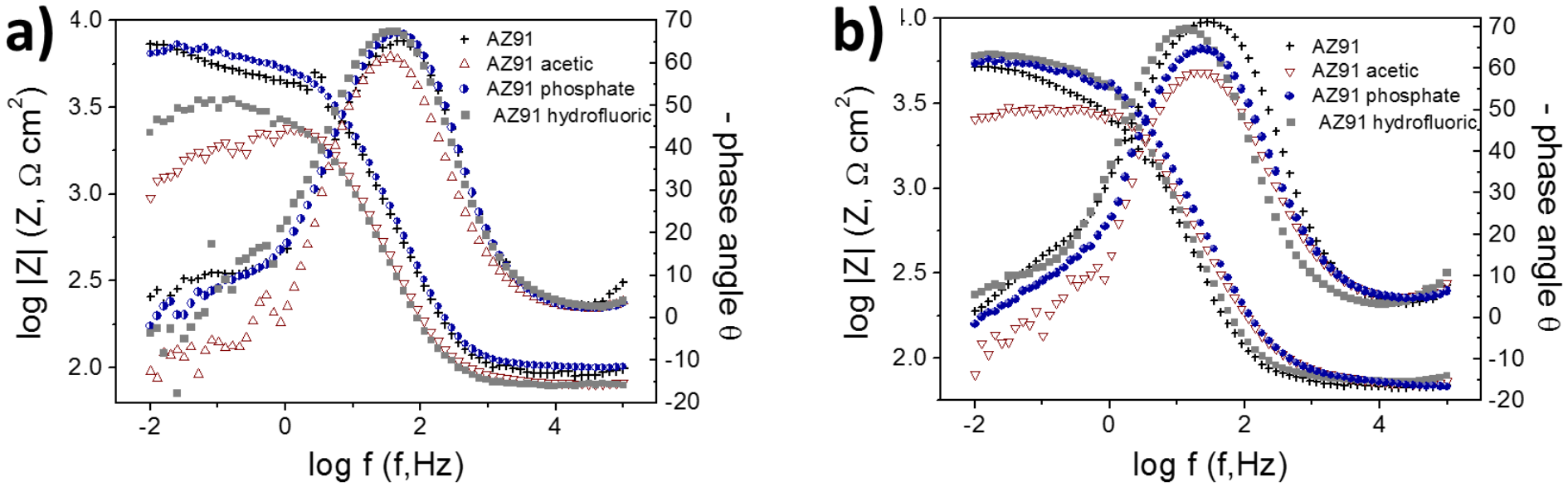
a)
b)
AZ91
AZ91 acetic
AZ91 phosphate
AZ91 hydrofluoric
log |Z| (Z, Ω cm^2)
- phase angle θ
log f (f,Hz)

Figure 5

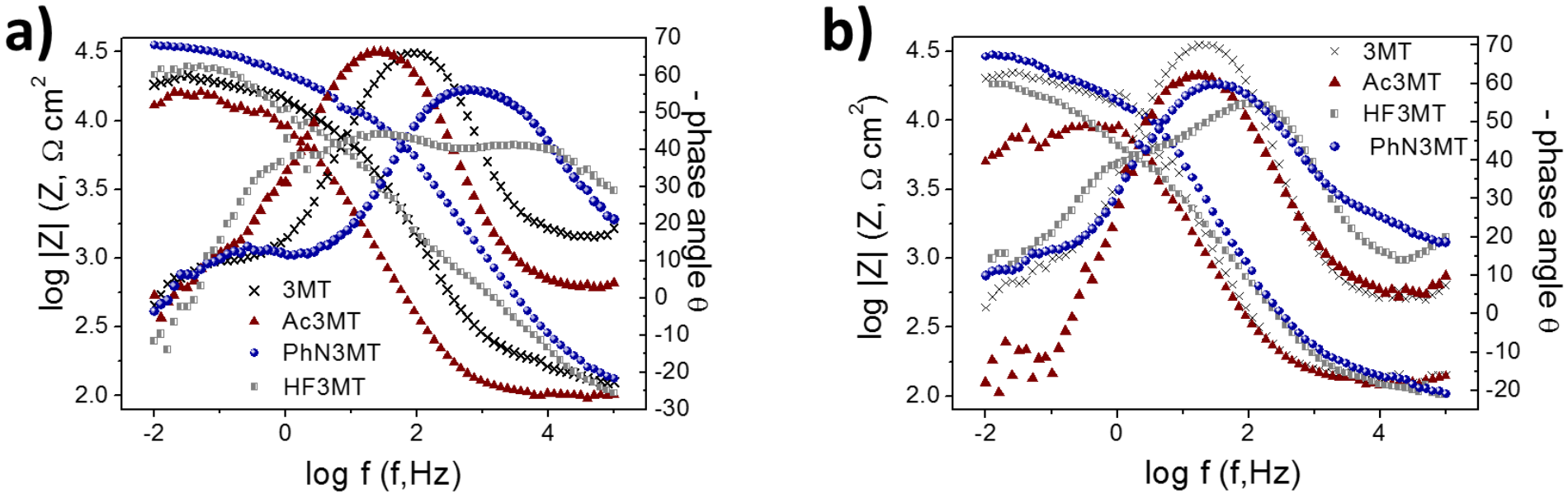

Figure 6

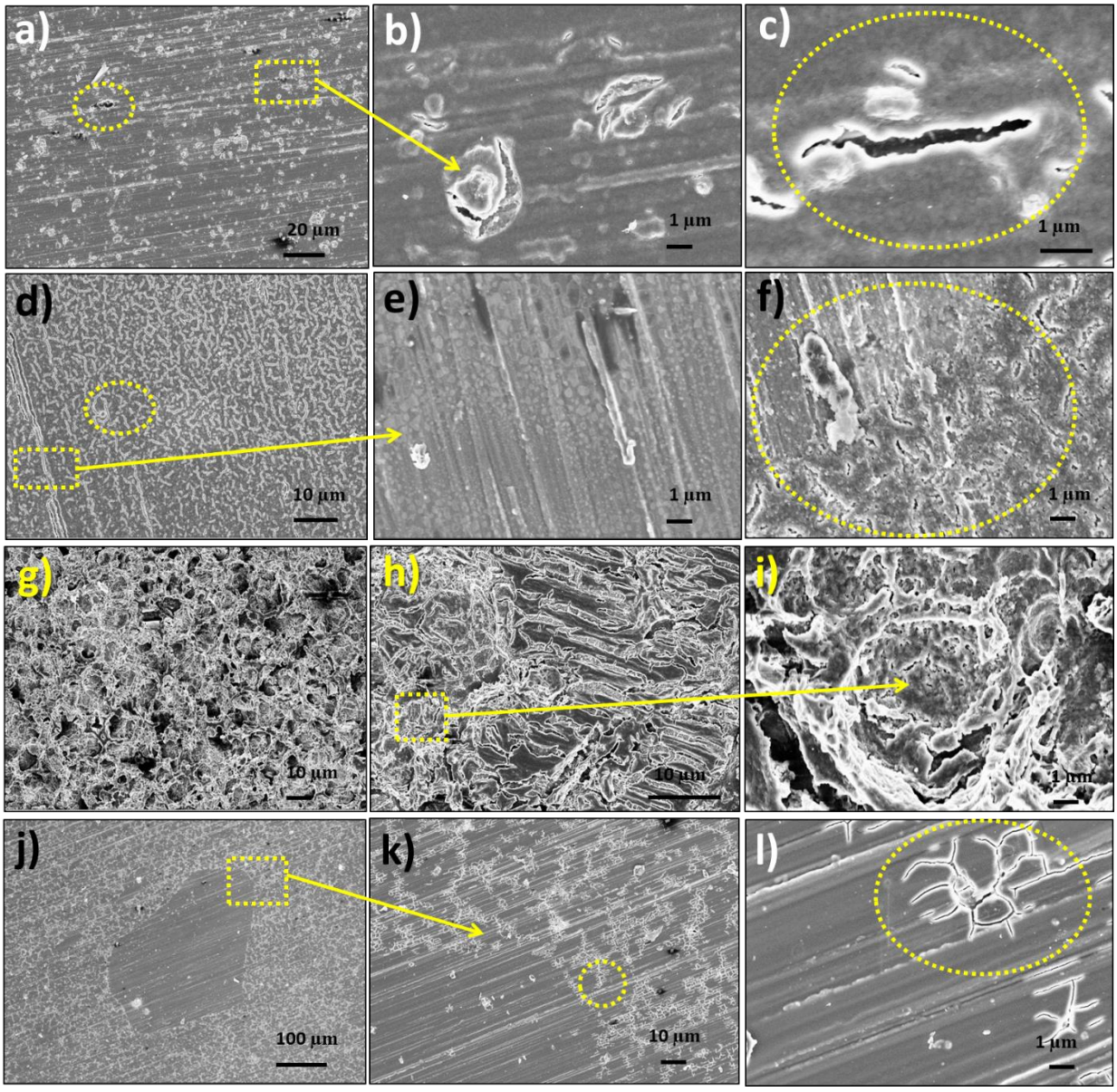
a)
20 µm
b)
1 µm
c)
1 µm
d)
10 µm
e)
1 µm
f)
1 µm
g)
10 µm
h)
10 µm
i)
1 µm
j)
100 µm
k)
10 µm
l)
1 µm

Figure 7

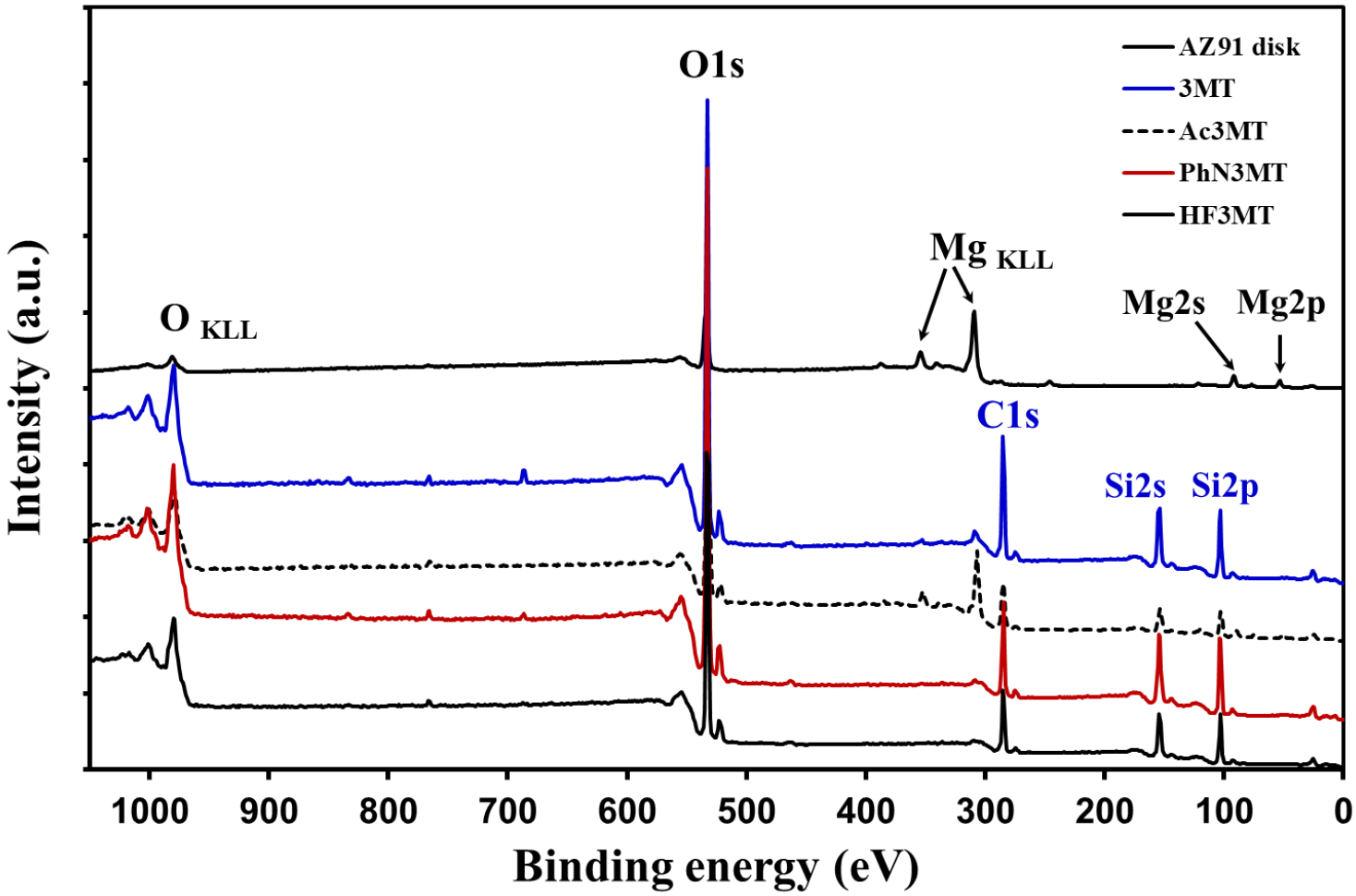
AZ91 disk
3MT
Ac3MT
PhN3MT
HF3MT
O1s
Mg KLL
O KLL
Mg2s
Mg2p
C1s
Si2s
Si2p
Intensity (a.u.)
1000
900
800
700
600
500
400
300
200
100
0
Binding energy (eV)

Figure 8

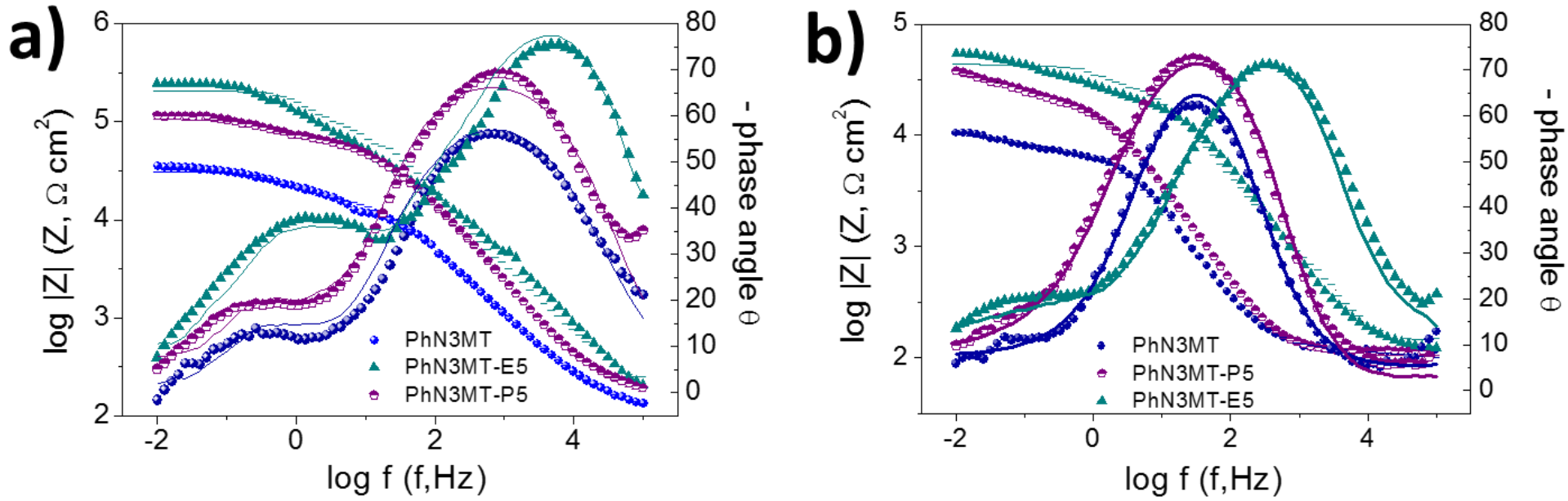
a)
log |Z| (Z, Ω cm²)
- phase angle θ
log f (f,Hz)
PhN3MT
PhN3MT-E5
PhN3MT-P5
b)
log |Z| (Z, Ω cm²)
- phase angle θ
log f (f,Hz)
PhN3MT
PhN3MT-P5
PhN3MT-E5

Figure 9

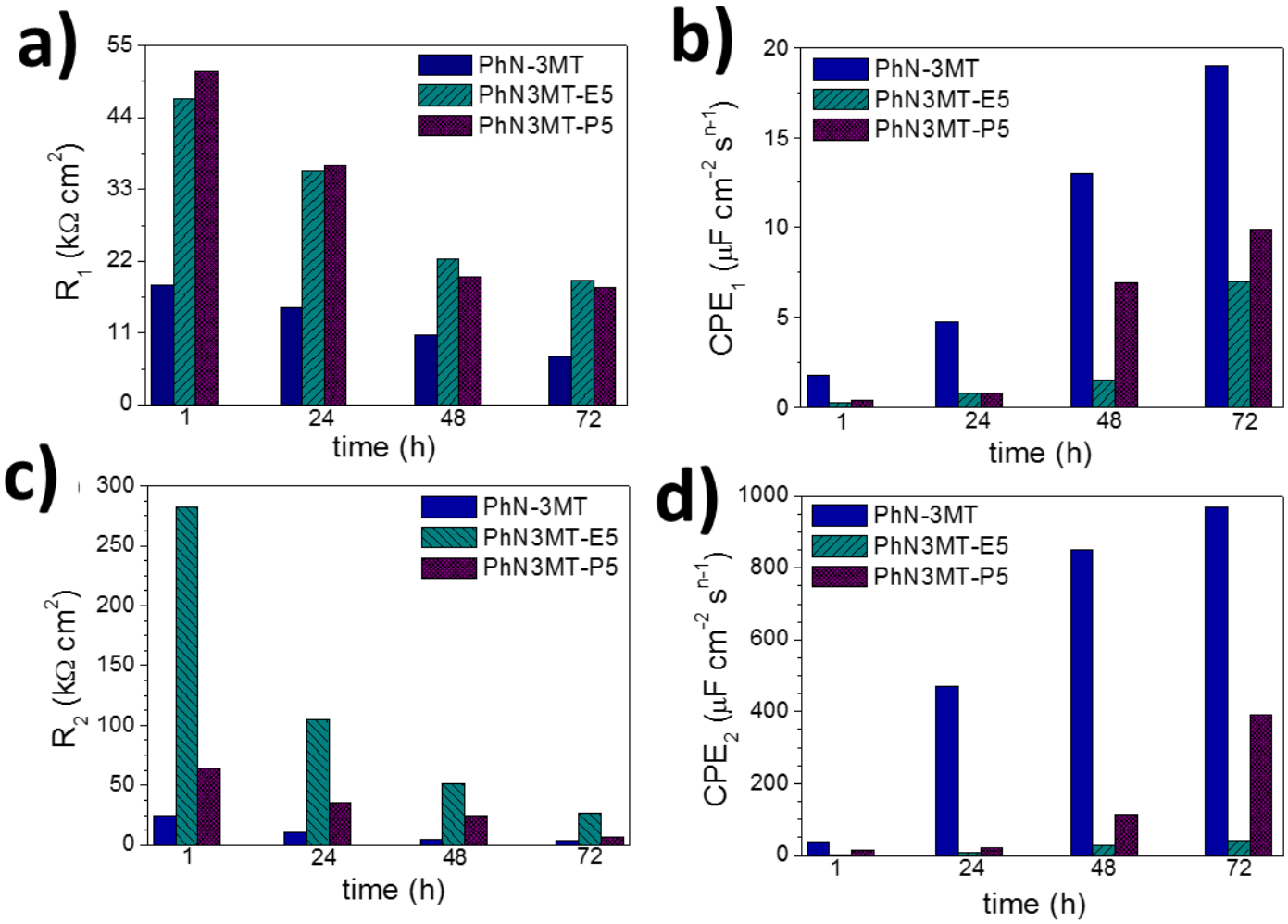
a)
b)
c)
d)
PhN-3MT
PhN3MT-E5
PhN3MT-P5
time (h)
R_1 (kΩ cm^2)
CPE_1 (μF cm^{-2} s^{n-1})
R_2 (kΩ cm^2)
CPE_2 (μF cm^{-2} s^{n-1})

Figure 10

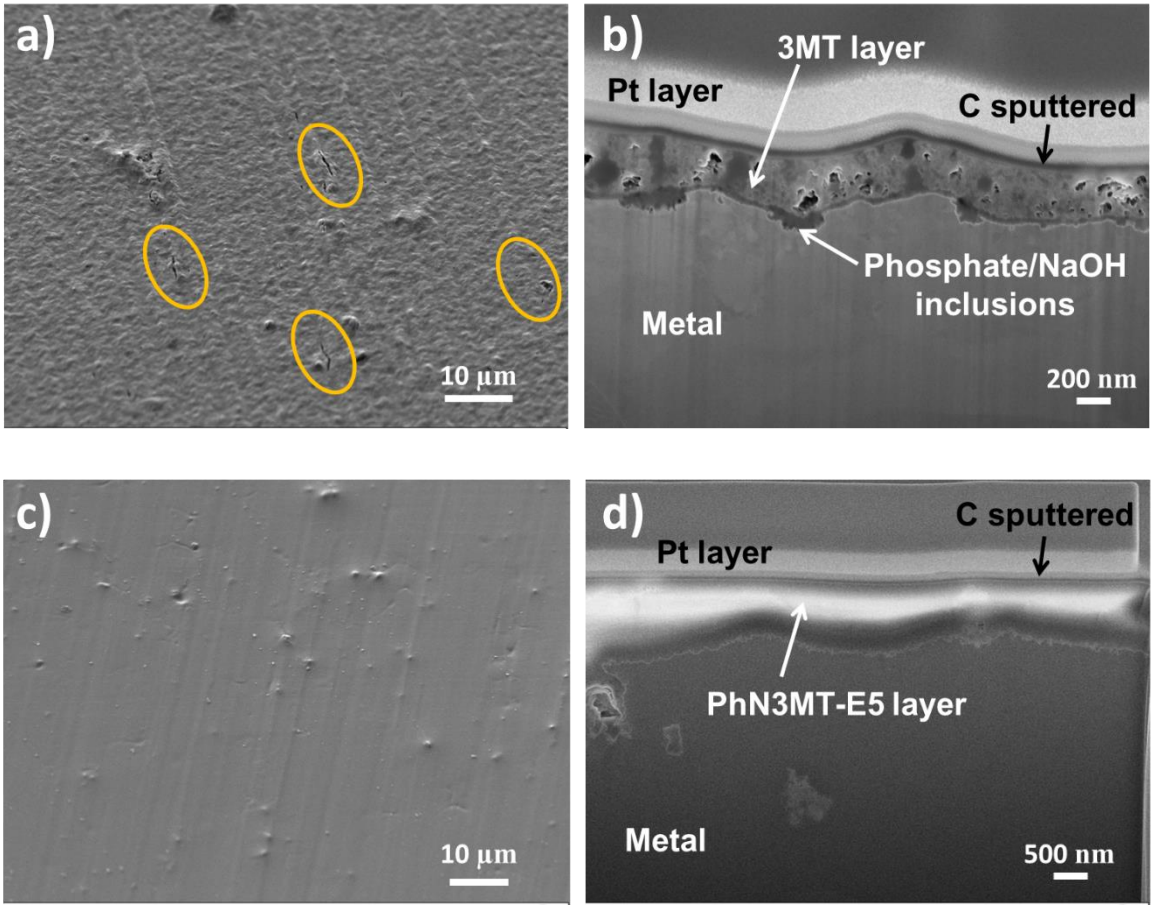
a)
10 µm
b)
3MT layer
Pt layer
C sputtered
Phosphate/NaOH
inclusions
Metal
200 nm
c)
10 µm
d)
C sputtered
Pt layer
PhN3MT-E5 layer
Metal
500 nm

Figure 11